

Radiative quark p_T -broadening in a quark-gluon plasma beyond the soft gluon approximation

B.G. Zakharov¹

¹*L.D. Landau Institute for Theoretical Physics, GSP-1, 117940, Kosygina Str. 2, 117334 Moscow, Russia*
(Dated: July 26, 2018)

We study the radiative correction to p_T -broadening of a fast quark in a quark-gluon plasma beyond the soft gluon approximation. We find that the radiative processes can suppress considerably p_T -broadening. This differs dramatically from previous calculations to logarithmic accuracy in the soft gluon approximation, predicting a considerable enhancement of p_T -broadening.

PACS numbers:

1. Interaction of fast partons with quark-gluon plasma (QGP) leads to jet modification in AA -collisions. It is dominated by radiative parton energy loss [1–7] due to parton multiple scattering in the QGP. The medium modification of jet fragmentation functions due to induced gluon emission leads to a strong suppression of hadron spectra in AA collisions at RHIC and LHC energies. It is characterized by the nuclear modification factor R_{AA} . In the last years the data on R_{AA} from RHIC and LHC have been actively used for tomographic analyses of the QGP produced in AA collisions. The suppression of particle spectra are related to modification of the jet parton distribution in the longitudinal (along the momentum of the initial hard parton) fractional momentum. Multiple parton scattering in the QGP can also modify the transverse jet distribution due to p_\perp -broadening of fast partons [3]. It should contribute to dijet and photon-jet angular decorrelation in AA collisions. Similarly to suppression of the hadron spectra, the observation of this effect could potentially give information on the density of the produced QCD matter.

For a single parton traversing a medium p_\perp -broadening is usually characterized by the transport coefficient \hat{q} [2, 3]: the mean squared momentum transfer for a gluon passing through a uniform medium of thickness L is $\langle p_\perp^2 \rangle = \hat{q}L$ (and for a quark $\langle p_\perp^2 \rangle = \hat{q}LC_F/C_A$). The radiative processes can give an additional contribution to p_\perp -broadening. The radiative contribution to $\langle p_\perp^2 \rangle$ has been addressed in recent papers [8–10]. It has been found that the radiative contribution may be rather large. It mostly comes from the double logarithmic term $\ln^2(L/l_0)$ (where l_0 is about the plasma Debye radius) [9]. The analyses [8–10] have been performed in the approximation of soft gluons. In the present letter we address radiative p_\perp -broadening beyond the soft gluon approximation and the logarithmic approximation used in [9]. We show that this reduces drastically the radiative contribution, that can even become negative. The analysis is based on the light-cone path integral (LCPI) [4] approach. The general LCPI formulas for p_\perp distribution in a $a \rightarrow bc$ transition have been obtained in [11] (see, also [12, 13], and [7] in the soft gluon limit).

2. We consider a fast quark with energy E produced at $z = 0$ (we choose the z -axis along the initial momentum

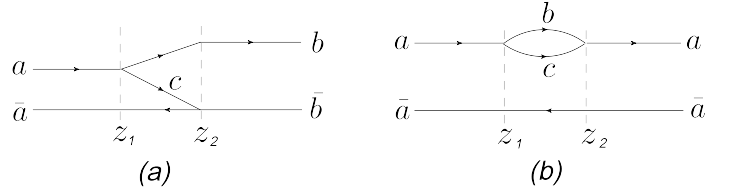


FIG. 1: Diagrammatic representation of $dP/dx_b d\mathbf{p}_\perp$ ($a \rightarrow bc$ process) (a) and of its virtual counterpart $d\tilde{P}/dx_b d\mathbf{p}_\perp$ ($a \rightarrow bc \rightarrow a$ process) (b). There are more two graphs with interexchange of vertices between the upper and lower lines.

of the quark) traversing a uniform medium of thickness L . We account for only single gluon emission. Then, the final states include the quark and the quark-gluon system. We neglect collisional energy loss (which is relatively small [14, 15]), then the energy of the final quark without gluon emission equals E . In this approximation the medium does not change the energy for the one- and two-body states. The presence of the medium modifies the relative fraction of the one-parton state and its transverse momentum distribution, and for the two-parton channel the medium modifies both the longitudinal and transverse momentum distributions. As in [9, 10], we will calculate the radiative correction to p_\perp -broadening of the final quark that includes both the one- and two-parton channels, i.e., irrespectively to the longitudinal quark energy loss for the qg -state. In this formulation the radiative contribution to $\langle p_\perp^2 \rangle$ reads

$$\langle p_\perp^2 \rangle_{rad} = \int dx_q d\mathbf{p}_\perp \mathbf{p}_\perp^2 \left[\frac{dP}{dx_q d\mathbf{p}_\perp} + \frac{d\tilde{P}}{dx_q d\mathbf{p}_\perp} \right], \quad (1)$$

where $\frac{dP}{dx_q d\mathbf{p}_\perp}$ is the distribution for real splitting $q \rightarrow qg$ in the transverse momentum of the final quark \mathbf{p}_\perp and its fractional longitudinal momentum x_q , $\frac{d\tilde{P}}{dx_q d\mathbf{p}_\perp}$ is the distribution for the virtual process $q \rightarrow qg \rightarrow q$. In the latter case x_q means the quark fractional momentum in the intermediate qg system, but \mathbf{p}_\perp , as for the real process, corresponds to the final quark. The x_q -integration in (1) can equivalently be written in terms of the gluon fractional momentum $x_g = 1 - x_q$. Below we will denote x_g as x .

Let us consider first the real splitting. In the LCPI approach the distribution on the transverse momentum and the longitudinal fractional momentum of the particle b has the form [11]

$$\frac{dP}{dx_b d\mathbf{p}_\perp} = \frac{1}{(2\pi)^2} \int d\boldsymbol{\tau}_f \exp(-i\mathbf{p}_\perp \boldsymbol{\tau}_f) F(\boldsymbol{\tau}_f), \quad (2)$$

where

$$F(\boldsymbol{\tau}_f) = 2\text{Re} \int_0^\infty dz_1 \int_{z_1}^\infty dz_2 \Phi_f(\boldsymbol{\tau}_f, z_2) \times \hat{g}K(\boldsymbol{\rho}_2, z_2 | \boldsymbol{\rho}_1, z_1) \Phi_i(\boldsymbol{\tau}_i, z_1) |_{\boldsymbol{\rho}_2=\boldsymbol{\tau}_f, \boldsymbol{\rho}_1=0}, \quad (3)$$

$$\Phi_i(\boldsymbol{\tau}_i, z_1) = \exp \left[-\frac{\sigma_{a\bar{a}}(\boldsymbol{\tau}_i)}{2} \int_0^{z_1} dz n(z) \right], \quad (4)$$

$$\Phi_f(\boldsymbol{\tau}_f, z_2) = \exp \left[-\frac{\sigma_{b\bar{b}}(\boldsymbol{\tau}_f)}{2} \int_{z_2}^\infty dz n(z) \right], \quad (5)$$

$\boldsymbol{\tau}_i = x_b \boldsymbol{\tau}_f$, $n(z)$ is the number density of the medium, $\sigma_{a\bar{a}}$ and $\sigma_{b\bar{b}}$ are the dipole cross sections for the $a\bar{a}$ and $b\bar{b}$ pairs, \hat{g} is the vertex operator, K is the Green function for the Hamiltonian

$$H = \frac{\mathbf{q}^2 + \epsilon^2}{2M} - \frac{in(z)\sigma_{\bar{a}bc}(\boldsymbol{\tau}_i, \boldsymbol{\rho})}{2}, \quad (6)$$

where $\mathbf{q} = -i\partial/\partial\boldsymbol{\rho}$, $M = E_a x_b x_c$, $\epsilon^2 = m_a^2 x_c + m_b^2 x_b - m_a^2 x_b x_c$ with $x_c = 1 - x_b$, and $\sigma_{\bar{a}bc}$ is the cross section for the three-body $\bar{a}bc$ system. The relative transverse parton positions for the $\bar{a}bc$ state read: $\boldsymbol{\rho}_{b\bar{a}} = \boldsymbol{\tau}_i + x_c \boldsymbol{\rho}$, $\boldsymbol{\rho}_{c\bar{a}} = \boldsymbol{\tau}_i - x_b \boldsymbol{\rho}$. The vertex operator in (3) acts on the Green function as

$$\hat{g}K(\boldsymbol{\rho}_2, z_2 | \boldsymbol{\rho}_1, z_1) = \frac{P_a^b(x_b)g(z_1)g(z_2)}{8\pi M^2} \times \frac{\partial}{\partial\boldsymbol{\rho}_1} \frac{\partial}{\partial\boldsymbol{\rho}_2} K(\boldsymbol{\rho}_2, z_2 | \boldsymbol{\rho}_1, z_1), \quad (7)$$

where $P_a^b(x_b)$ is the standard $a \rightarrow b$ splitting function. Note that the derivatives on the right-hand side of (7) should be calculated for a fixed $\boldsymbol{\tau}_i$, i.e. for a fixed position of the center mass of the bc pair. The formula (7) is written for z -dependent coupling constant g , because the z -integrations in (3) extend up to infinity, and the adiabatically vanishing coupling should be used.

Diagrammatically, $\frac{dP}{dx_b d\mathbf{p}_\perp}$ is shown in Fig. 1a. The initial and final parallel lines in Fig. 1 correspond to the Glauber factors (4) and (5), and the three-body part between z_1 and z_2 corresponds to the Green function of the Hamiltonian (6). The factor 2 in (3) accounts for the contribution from the diagram that can be obtained from Fig. 1a by interexchange of the vertices between the upper and lower lines. Diagram representation for the virtual process $a \rightarrow bc \rightarrow a$ that defines $\frac{d\hat{P}}{dx_b d\mathbf{p}_\perp}$ is shown

in Fig. 1b. In the virtual counterpart of (3) $\boldsymbol{\tau}_i = \boldsymbol{\tau}_f$, and the three-body part also corresponds to the Green function (but now with arguments $\boldsymbol{\rho}_1 = \boldsymbol{\rho}_2 = 0$) of the Hamiltonian (6). The vertex factor for the virtual process changes sign.

For $q \rightarrow qg$ splitting (i.e. when $a = q$, $b = q$, $c = g$) the three-body cross section reads [16]

$$\sigma_{\bar{q}qg} = \frac{9}{8} [\sigma_2(\boldsymbol{\rho}_{qg}) + \sigma_2(\boldsymbol{\rho}_{g\bar{q}})] - \frac{1}{8} \sigma_2(\boldsymbol{\rho}_{q\bar{q}}), \quad (8)$$

where σ_2 is the dipole cross section for the $q\bar{q}$ system. We will use the quadratic approximation

$$\sigma_2(\rho) = C\rho^2, \quad C = \hat{q}C_F/2C_{An}. \quad (9)$$

In this case the Hamiltonian (6) can be written in the oscillator form, for which one can use the analytical formula for the Green function.

At zero density the Glauber factors $\Phi_{i,f}$ become equal to unity, and the Green function is reduced to the vacuum one

$$K_0(\boldsymbol{\rho}_2, z_2 | \boldsymbol{\rho}_1, z_1) = \frac{M}{2\pi i(z_2 - z_1)} \times \exp \left\{ i \left[\frac{M(\boldsymbol{\rho}_2 - \boldsymbol{\rho}_1)^2}{2(z_2 - z_1)} - \frac{\epsilon^2(z_2 - z_1)}{2M} \right] \right\}. \quad (10)$$

At any fixed z_1

$$\text{Re} \int_{z_1}^\infty dz_2 K_0(\boldsymbol{\rho}_2, z_2 | \boldsymbol{\rho}_1, z_1) = 0. \quad (11)$$

However, the integration over z_1 in (3) is unconstrained, and for a fixed coupling one gets the indeterminate product $0 \times \infty$. It can be resolved, using the exponentially decreasing coupling

$$g(z) = g \exp(-\delta z), \quad (12)$$

and taking the limit $\delta \rightarrow 0$ after the $z_{1,2}$ -integration. This $\delta \rightarrow 0$ limit procedure gives for $n = 0$ the standard spectrum for $q \rightarrow qg$ splitting in vacuum

$$\frac{dP_0}{dx d\mathbf{p}_\perp} = \frac{\alpha_s C_F}{2\pi^2 x} [1 + (1-x)^2] \frac{\mathbf{p}_\perp^2}{(\mathbf{p}_\perp^2 + \epsilon^2)^2}. \quad (13)$$

For a nonzero density the z -integrals in (3) over the region $z_{1,2} > L$ also can be expressed via the vacuum spectrum. To separate this contribution it is convenient to write the product $\Phi_f(\boldsymbol{\tau}_f, z_2) \hat{g}K(\boldsymbol{\rho}_2, z_2 | \boldsymbol{\rho}_1, z_1) \Phi_i(\boldsymbol{\tau}_i, z_1)$ in the integrand function on the right-hand side of (3) as (we denote $\hat{g}K$ as \mathcal{K} and omit arguments for notational simplicity)

$$\Phi_f \mathcal{K} \Phi_i = \Phi_f (\mathcal{K} - \mathcal{K}_0) \Phi_i + (\Phi_f - 1) \mathcal{K}_0 \Phi_i + \mathcal{K}_0 (\Phi_i - 1) + \mathcal{K}_0. \quad (14)$$

The last term on the right-hand side of (14) just corresponds to the vacuum splitting. It can be omitted because it does not contain medium effects.

The Green function K in the oscillator approximation, similarly to the vacuum one (10), is the exponential of a quadratic form of the transverse vectors $\boldsymbol{\rho}_{1,2}$. In this case, each of the medium dependent terms in (14) is a combination of terms of the types $\exp(-\boldsymbol{\tau}_f^2 A)$ and $\boldsymbol{\tau}_f^2 \exp(-\boldsymbol{\tau}_f^2 A)$, and, for given values of $z_{1,2}$ the $\boldsymbol{\tau}_f$ integration in (2) becomes Gaussian. It allows one to represent the \mathbf{p}_\perp -distribution (2) via the $z_{1,2}$ -integrals [11]. However, for derivation of the $\langle p_\perp^2 \rangle$ the explicit form of the \mathbf{p}_\perp -distribution is unnecessary. Because from (2) it is clear that it may be written as the Laplacian ∇^2 of the function F at $\boldsymbol{\tau}_f = 0$. The Laplacian for the first three terms on the right-hand side of (14), that we need for calculation of $\nabla^2 F$ at $\boldsymbol{\tau}_f = 0$, read

$$\nabla^2[\Phi_f(\mathcal{K} - \mathcal{K}_0)\Phi_i] = \nabla^2\Phi_f(\mathcal{K} - \mathcal{K}_0) + (\mathcal{K} - \mathcal{K}_0)\nabla^2\Phi_i + \nabla^2(\mathcal{K} - \mathcal{K}_0), \quad (15)$$

$$\nabla^2[(\Phi_f - 1)\mathcal{K}_0\Phi_i] = \nabla^2\Phi_f\mathcal{K}_0, \quad (16)$$

$$\nabla^2[\mathcal{K}_0(\Phi_i - 1)] = \mathcal{K}_0\nabla^2\Phi_i. \quad (17)$$

The total $\langle p_\perp^2 \rangle_{rad}$ (1) includes also the contribution of the virtual diagrams. As in (1) we will denote the quantities for the virtual diagrams with a tilde. The real and virtual final Glauber factors Φ_f and $\tilde{\Phi}_f$ are equal. Because they depend on the $\boldsymbol{\tau}_f$, which is same for real and virtual graphs. For this reason the virtual contribution will cancel the contributions for the real process in (15) and (16) that contain $\nabla^2\Phi_f$ (if we account for the fact that $\mathcal{K} = -\tilde{\mathcal{K}}$ and $\mathcal{K}_0 = -\tilde{\mathcal{K}}_0$ at $\boldsymbol{\tau}_f = 0$). However, the terms with $\nabla^2\Phi_i$ in (15) and (17) are not canceled by the contributions from the virtual diagrams. Because the argument $\boldsymbol{\tau}_i$ has different values for the initial state Glauber factors for the real and virtual splitting: $\boldsymbol{\tau}_i = (1-x)\boldsymbol{\tau}_f$ for the real case and $\boldsymbol{\tau}_i = \boldsymbol{\tau}_f$ for the virtual one. Then, the total $\langle p_\perp^2 \rangle_{rad}$, corresponding to the sum $F + \tilde{F}$, can be written as

$$\langle p_\perp^2 \rangle_{rad} = I_1 + I_2 + I_3, \quad (18)$$

$$I_1 = 2\text{Re} \int dx \int_0^L dz_1 \int_0^\infty dz_{21} \nabla^2(\mathcal{K} - \mathcal{K}_0 + \tilde{\mathcal{K}} - \tilde{\mathcal{K}}_0), \quad (19)$$

$$\begin{aligned} I_2 &= 2\text{Re} \int dx \int_0^L dz_1 \int_0^\infty dz_{21} [(\mathcal{K} - \mathcal{K}_0)\nabla^2\Phi_i \\ &\quad + (\tilde{\mathcal{K}} - \tilde{\mathcal{K}}_0)\nabla^2\tilde{\Phi}_i] \\ &= -2\langle p_\perp^2 \rangle_0 \text{Re} \int dx f(x) \int_0^L dz_1 \frac{z_1}{L} \int_0^\infty dz_{21} (\mathcal{K} - \mathcal{K}_0), \quad (20) \end{aligned}$$

$$\begin{aligned} I_3 &= 2\text{Re} \int dx \int_0^\infty dz_1 \int_0^\infty dz_{21} [\mathcal{K}_0\nabla^2\Phi_i + \tilde{\mathcal{K}}_0\nabla^2\tilde{\Phi}_i] \\ &= -2\text{Re} \int dx f(x) \int_0^\infty dz_1 \int_0^\infty dz_{21} \mathcal{K}_0\nabla^2\tilde{\Phi}_i \quad (21) \end{aligned}$$

with $f(x) = x(2-x)$, and $z_{21} = z_2 - z_1$. As in (14)–(17), we omit arguments for simplicity. In (19)–(21) all the functions in the integrands should be calculated at $\boldsymbol{\tau}_f = 0$. The last lines in (20) and (21) used the fact that at $\boldsymbol{\tau}_f = 0$ $\mathcal{K} = -\tilde{\mathcal{K}}$, $\mathcal{K}_0 = -\tilde{\mathcal{K}}_0$, $\nabla^2\Phi_i = (1-x)^2\nabla^2\tilde{\Phi}_i$, and $\nabla^2\tilde{\Phi}_i$ equals $\langle p_\perp^2 \rangle_0 z_1/L$, where $\langle p_\perp^2 \rangle_0$ corresponds to nonradiative p_\perp -broadening.

The integrations over z_1 in (19) and (20) are constrained by $z_1 = L$, because $\mathcal{K} - \mathcal{K}_0$ and $\tilde{\mathcal{K}} - \tilde{\mathcal{K}}_0$ vanish at $z_1 > L$. Note that it can be carried out setting $\delta = 0$ in (12). However, the integration over $z_{1,2}$ in (21), similarly to calculation of the vacuum spectrum (13), is unconstrained, and should be performed for a finite δ , and then taking the limit $\delta \rightarrow 0$. The $\delta \rightarrow 0$ limit procedure allows to represent (21) in the form

$$I_3 = -\langle p_\perp^2 \rangle_0 \int dx f(x) \frac{dP_0}{dx}, \quad (22)$$

where

$$\frac{dP_0}{dx} = \int d\mathbf{p}_\perp \frac{dP_0}{dx d\mathbf{p}_\perp} \quad (23)$$

is the \mathbf{p}_\perp -integrated vacuum spectrum (13). The \mathbf{p}_\perp -integral in (23) is logarithmically divergent. This occurs because the formula (2) is obtained in the small angle approximation [11], and ignores the kinematic limits. We regulate (23) by restricting the integration region to $p_\perp < p_\perp^{max}$ with $p_\perp^{max} = E \min(x, (1-x))$. Formally, this divergence may be regulated by introduction of the Pauli-Villars counter term with ϵ replaced by $\epsilon' \sim p_\perp^{max}$.

The z_{21} -integral in (19) is also logarithmically divergent, because the integrand behaves as $1/z_{21}$ when $z_{21} \rightarrow 0$. Similarly to the logarithmic divergence of the p_\perp -integration for I_3 , this divergence is a consequence of the small angle approximation. And it also can be regulated by the Pauli-Villars counter terms with $\epsilon' \sim p_\perp^{max}$. Such counter terms will suppress the integrand at $z_{21} \lesssim M/\epsilon'^2$ (for small x it is equivalent to $z_{21} \lesssim 1/\omega$). However, this would be reasonable only for a medium with a vanishing longitudinal correlation size. For the real QGP with the correlation radius $\sim 1/m_D$ (here m_D is Debye mass for the QGP) the medium effect on the diagrams shown in Fig. 1 should vanish when z_{21} becomes small as compared to the Debye radius. For this reason it is reasonable to regulate the z_{21} -integral in (19) by using the lower limit $z_{21} \sim 1/m_D$ (that is bigger than $1/\omega$ at $\omega \gg m_D$). This prescription has been used in [9] for calculation in the logarithmic approximation of the contribution corresponding to our I_1 (19). It was found that the dominating contribution comes from the double logarithmic term $\propto \ln^2(L/l_0)$ with l_0 the minimum z_{21} . The contributions from I_2 and I_3 terms have not

been included in [9]. As will be seen below, these terms turn out to be very important, because they are negative and comparable to I_1 . As a result, they change $\langle p_{\perp}^2 \rangle_{rad}$ drastically.

3. To make estimates of $\langle p_{\perp}^2 \rangle_{rad}$ we use the quasiparticle masses $m_q = 300$ and $m_g = 400$ MeV [17], that have been used in our previous analyses [18, 19] of the RHIC and LHC data on the nuclear modification factor R_{AA} . The calculations of [18, 19] have been performed for a more sophisticated model. In [18, 19] the induced gluon emission has been calculated with running α_s for the QGP with Bjorken's longitudinal expansion, which corresponds to $\hat{q} \propto 1/\tau$. In the present analysis, as in [9], we use constant \hat{q} and α_s . To make our estimates as accurate as possible we adjusted the value of \hat{q} to reproduce the quark energy loss ΔE for running α_s in the model of [19] with the Debye mass from the lattice calculations [20]. As in [9], we take $\alpha_s = 1/3$ and $L = 5$ fm. We obtained $\hat{q} \approx 0.27$ GeV³ at $E = 30$ GeV for Au+Au collisions at $\sqrt{s} = 0.2$ TeV and $\hat{q} \approx 0.32$ GeV³ at $E = 100$ GeV for Pb+Pb collisions at $\sqrt{s} = 2.76$ TeV.

From the point of view of the numerical predictions for $\langle p_{\perp}^2 \rangle_{rad}$ within the oscillator approximation (9), it is important that the transport coefficient is an energy dependent quantity. The energy dependence appears due to the Coulomb effects. To a good approximation \hat{q} can be written as [3, 21, 22]

$$\hat{q} = n \int_0^{p_{\perp}^2 max} dp_{\perp}^2 p_{\perp}^2 \frac{d\sigma}{dp_{\perp}^2} \quad (24)$$

with $p_{\perp}^2 max \sim 3\omega T$, ω the gluon energy, T the QGP temperature, $d\sigma/dp_{\perp}^2$ the differential gluon cross section. The p_{\perp}^2 -integration in (24) is logarithmic, and for this reason \hat{q} has a weak energy dependence. The induced gluon emission is dominated by radiation of soft gluons with $x \ll 1$. The typical gluon energy, $\bar{\omega}$, is small compared to the initial quark energy, and depends weakly on E [23]. At $x \ll 1$ the induced gluon emission is dominated by the gluon multiple scattering. For this reason, the induced gluon spectrum is controlled by the value of the transport coefficient for soft gluons. Since the energy dependence of \hat{q} is weak, it can be calculated at $\omega \sim \bar{\omega}$. In the case of interest, $\bar{\omega} \sim 3 - 5$ GeV for a quark with $E \sim 30 - 100$ GeV. The above adjusted values of \hat{q} correspond just to the transport coefficients for gluons with energy $\sim \bar{\omega}$. However, the Glauber factors Φ_i and $\tilde{\Phi}_i$, that enter (20) and (21), correspond to the initial quark, and they should be calculated with the transport coefficient at energy E . We will denote it as \hat{q}' , leaving the notation \hat{q} for the transport coefficient at $\bar{\omega}$. Since $E \gg \bar{\omega}$, the ratio $r = \hat{q}'/\hat{q}$ may differ significantly from unity. With the help of the formula (24) using the Debye mass from [20] and running α_s parametrized as in our

previous jet quenching analysis [19] we obtained

$$r \approx 2.4(2.63) \quad (25)$$

at $E = 30(100)$ GeV for quark jets for RHIC(LHC) conditions.

In numerical calculations in (20)–(21) we integrate over x from $x_{min} = m_g/E$ to $x_{max} = 1 - m_q/E$. As in [9], for the cutoff in the z_{21} -integration we use $z_{21}^{min} = 1/m$ with $m = 300$ MeV. For the three terms in (18) we obtained

$$[I_1, I_2, I_3]/\langle p_{\perp}^2 \rangle_0 \approx [0.436/r, -0.213, -0.601] \quad (26)$$

at $E = 30$ GeV for the RHIC conditions, and

$$[I_1, I_2, I_3]/\langle p_{\perp}^2 \rangle_0 \approx [0.85/r, -0.107, -0.908] \quad (27)$$

at $E = 100$ GeV for the LHC conditions. Using (25) we obtain from (26) and (27) for our RHIC(LHC) versions

$$\langle p_{\perp}^2 \rangle_{rad}/\langle p_{\perp}^2 \rangle_0 \approx -0.632(-0.692), \quad r = 2.4(2.63). \quad (28)$$

And if we ignore the difference between \hat{q}' and \hat{q}

$$\langle p_{\perp}^2 \rangle_{rad}/\langle p_{\perp}^2 \rangle_0 \approx -0.378(-0.165), \quad r = 1(1). \quad (29)$$

One sees that in all the cases the radiative contribution to the mean squared p_{\perp} is negative. This differs drastically from the prediction of [9] $\langle p_{\perp}^2 \rangle_{rad} \approx 0.75\hat{q}L$. In the form used in (28), (29) it reads $\langle p_{\perp}^2 \rangle_{rad}/\langle p_{\perp}^2 \rangle_0 \approx 0.75 \frac{C_A}{rC_F} \approx 1.7/r$. The negative values of (28), (29) are due to a large negative contribution from $I_{2,3}$. Since these terms have not been accounted for in [9], it is interesting to compare prediction of [9] with our results for I_1 term alone. From (26) and (27) one can see that our $\langle p_{\perp}^2 \rangle_{rad}|_{I_1}$ is smaller than $\langle p_{\perp}^2 \rangle_{rad}$ from [9] by a factor of $\sim 3.9(2)$ for the RHIC(LHC) cases. This discrepancy says that the logarithmic approximation used in [9] is rather crude.

Thus, we have found that the radiative contribution to p_{\perp} -broadening may be negative, or at least strongly suppressed as compared to the predictions of [9, 10]. This seems to be supported by the recent STAR measurement of the hadron-jet correlations [24], in which no evidence for large-angle jet scattering in the medium has been found. Similar to the analyses of [9, 10], our calculations are performed for a uniform medium in the oscillator approximation. It would be interesting to perform calculations for an expanding QGP, and to go beyond the oscillator approximation. We leave it for future work. Of course, it is highly desirable to study the higher order effects. However, even in the oscillator approximation and for a uniform medium, such calculations are extremely difficult [25].

This work has been supported by the RScF grant 16-12-10151.

[1] M. Gyulassy and X.N. Wang, Nucl. Phys. B**420**, 583 (1994) [nucl-th/9306003].

[2] R. Baier, Y.L. Dokshitzer, A.H. Mueller, S. Peigné

- and D. Schiff, Nucl. Phys. B**483**, 291 (1997) [hep-ph/9607355].
- [3] R. Baier, Y.L. Dokshitzer, A.H. Mueller, S. Peigné and D. Schiff, Nucl. Phys. B**484**, 265 (1997) [hep-ph/9608322].
- [4] B.G. Zakharov, JETP Lett. **63**, 952 (1996) [hep-ph/9607440]; Phys. Atom. Nucl. **61**, 838 (1998) [hep-ph/9807540].
- [5] M. Gyulassy, P. Lévai and I. Vitev, Nucl. Phys. B**594**, 371 (2001) [hep-ph/0006010].
- [6] P. Arnold, G.D. Moore and L.G. Yaffe, JHEP **0206**, 030 (2002) [hep-ph/0204343].
- [7] U.A. Wiedemann, Nucl. Phys. A**690**, 731 (2001) [hep-ph/0008241].
- [8] B. Wu, JHEP **1110**, 029 (2011) [arXiv:1102.0388].
- [9] T. Liou, A.H. Mueller and B. Wu, Nucl. Phys. A**916**, 102 (2013) [arXiv:1304.7677].
- [10] J.-P. Blaizot and Y. Mehtar-Tani, Nucl. Phys. A**929**, 202 (2014) [arXiv:1403.2323].
- [11] B.G. Zakharov, JETP Lett. **70**, 176 (1999) [hep-ph/9906536].
- [12] R. Baier, D. Schiff and B.G. Zakharov, Ann. Rev. Nucl. Part. Sci. **50**, 37 (2000) [hep-ph/0002198].
- [13] B.G. Zakharov, Nucl. Phys. Proc. Suppl. **146**, 151 (2005) [hep-ph/0412117].
- [14] B.G. Zakharov, JETP Lett. **86**, 444 (2007) [arXiv:0708.0816].
- [15] G.-Y. Qin, J. Ruppert, C. Gale, S. Jeon, G.D. Moore and M.G. Mustafa, Phys. Rev. Lett. **100**, 072301 (2008) [arXiv:0710.0605].
- [16] N.N. Nikolaev, B.G. Zakharov and V.R. Zoller, JETP Lett. **59**, 6 (1994) [hep-ph/9312268].
- [17] P. Lévai and U. Heinz, Phys. Rev. C**57**, 1879 (1998).
- [18] B.G. Zakharov, J. Phys. G**40**, 085003 (2013) [arXiv:1304.5742].
- [19] B.G. Zakharov, J. Phys. G**41**, 075008 (2014) [arXiv:1311.1159].
- [20] O. Kaczmarek and F. Zantow, Phys. Rev. D**71**, 114510 (2005) [hep-lat/0503017].
- [21] K.M. Burke *et al.* [JET Collaboration] Phys. Rev. C**90**, 014909 (2014) [arXiv:1312.5003].
- [22] R. Baier, Nucl. Phys. A**715**, 209 (2003) [hep-ph/0209038].
- [23] B.G. Zakharov, JETP Lett. **73**, 49 (2001) [hep-ph/0012360].
- [24] L. Adamczyk *et al.* [STAR Collaboration], Phys.Rev. C**96**, 024905 (2017) [arXiv:1702.01108].
- [25] P. Arnold and S. Iqbal, JHEP **1504**, 070 (2015), Erratum: JHEP **1609**, 072 (2016) [arXiv:1501.04964]; [arXiv:1806.08796].